Limits on Exotic Long-Range Spin-Spin Interactions of Electrons

B. R. Heckel, W. A. Terrano, and E. G. Adelberger[*]

*Center for Experimental Nuclear Physics and Astrophysics, Box 354290, University of Washington,
Seattle, Washington 98195-4290, USA*
(Received 1 August 2013; published 10 October 2013)

We surrounded a rotating torsion pendulum containing 9.8×10^{22} polarized electrons by 2 or 4 stationary sources, each with a net spin of 6.0×10^{24} polarized electrons. Multiple source configurations gave sensitivity to hypothetical dipole-dipole, spin-dot-spin, and spin-cross-spin exchange interactions mediated by bosons with masses up to 20 μeV. For bosons with masses ≤ 0.1 μeV our null results for the dipole-dipole, spin-dot-spin, and spin-cross-spin forces imply 1σ upper limits on $(g_P^e)^2/(\hbar c)$, $(g_A^e)^2/(\hbar c)$ and $(g_V^e g_A^e)/(\hbar c)$ of 2.2×10^{-16}, 3.8×10^{-40}, and 1.2×10^{-28}, respectively. We also constrain, for the first time, any possible linear combination of static spin-spin interactions. In this case our upper limits relax to 5.6×10^{-16}, 9.8×10^{-40}, and 1.2×10^{-28}, respectively.

Many extensions of the standard model predict new massless or ultra-low-mass bosons that could be detected via the macroscopic forces that they mediate. Conventional "gravitational" experiments strongly constrain exotic spin-independent forces arising from scalar or vector interactions that couple to unpolarized bodies [1]. Considerably less theoretical and experimental attention has been devoted to spin-dependent forces that, in first order, act only between spin-polarized bodies. Such exchange forces would be produced by bosons with pseudoscalar or axial vector couplings. Moody and Wilczek [2] and Dobrescu and Mocioiu [3] enumerated the potentials that can arise from one-boson exchange, constrained only by rotational and translational invariance, while Kostelecký and co-workers [4] have considered spin-dependent interactions that could arise in general preferred-frame scenarios.

We have previously used a rotating torsion balance to constrain velocity-independent and velocity-dependent interactions between the polarized electrons in a "spin pendulum" and unpolarized terrestrial and astronomical bodies [5], and employed an instrument with a stationary, unpolarized torsion pendulum surrounded by polarized electrons in a ferromagnet to constrain the monopole-dipole interaction of axionlike particles [6].

Here we report constraints on interactions between the polarized electrons in our pendulum and polarized electrons in stationary laboratory sources that employ the same technology used in the spin pendulum. Our results are sensitive to all 3 velocity-independent, spin-spin potentials discussed in Ref. [3] that can be mediated by spin-1 bosons with axial and vector couplings g_A and g_V:

$$V_1 = \frac{g_A^2}{4\pi r}(\hat{\boldsymbol{\sigma}}_1 \cdot \hat{\boldsymbol{\sigma}}_2)e^{-r/\lambda}; \tag{1}$$

$$V_2 = -\frac{g_A g_V \hbar}{4\pi m_e c r^2}(\hat{\boldsymbol{\sigma}}_1 \times \hat{\boldsymbol{\sigma}}_2 \cdot \hat{\boldsymbol{r}})\left(1 + \frac{r}{\lambda}\right)e^{-r/\lambda} \tag{2}$$

and

$$V_3 = -\frac{(g_A^2 + g_V^2)\hbar^2}{16\pi m_e^2 c^2 r^3}[(\hat{\boldsymbol{\sigma}}_1 \cdot \hat{\boldsymbol{\sigma}}_2)\left(1 + \frac{r}{\lambda}\right)$$
$$- (\hat{\boldsymbol{\sigma}}_1 \cdot \hat{\boldsymbol{r}})(\hat{\boldsymbol{\sigma}}_2 \cdot \hat{\boldsymbol{r}})\left(3 + \frac{3r}{\lambda} + \frac{r^2}{\lambda^2}\right)]e^{-r/\lambda}; \tag{3}$$

where $\boldsymbol{r} = \boldsymbol{r}_1 - \boldsymbol{r}_2$ and $\lambda = \hbar/(m_b c)$ is the interaction range associated with bosons of mass m_b. V_3, the familiar dipole-dipole interaction, can also result from a pseudoscalar interaction; in that case the pseudoscalar coupling constant g_P^2 replaces $(g_A^2 + g_V^2)$. Pseudoscalars are of particular theoretical interest: any theory with a broken high-energy symmetry generates Goldstone bosons that couple to fermions via $(1/F)\partial_\mu \phi \bar{\psi} \gamma^\mu \gamma_5 \psi$ where F is the symmetry-breaking scale and ψ is the fermion field. This is identical [7] to a pseudoscalar interaction with $g_P \approx m_e/F$. Additionally, extensions of general relativity to include torsion typically predict a propagating torsion field that behaves like a pseudoscalar [8].

Our rotating torsion balance, the spin pendulum, and data-taking procedures have already been described in detail [5]. The spin pendulum contains $\sim 9.8 \times 10^{22}$ polarized electrons but has a negligible external magnetic field. This was achieved by combining SmCo$_5$ and Alnico permanent magnets, magnetized to the same degree, so that the B fields nominally form closed loops with no external flux. The electron spins, however, do not form closed loops because the spin density of SmCo$_5$ at a given magnetization is about half that of Alnico (a large orbital contribution to the magnetic moment nearly cancels the spin moment; see Ref. [5] for details). The pendulum was surrounded by four layers of magnetic shielding to isolate it from external magnetic fields, and the entire balance was rotated continuously with a period of about 20 minutes to modulate the pendulum's spin orientation relative to the lab. Note that we probe interactions that couple to spin and not to charge
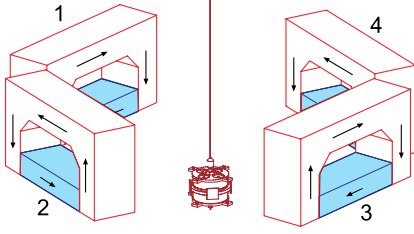
FIG. 1 (color online).   Scale drawing of the spin pendulum and spin sources in configuration 4H. The shaded blue bars of the sources are $SmCo_5$ and the unshaded red pieces are magnet iron. The bottoms of the source cores were 2.6 cm above the pendulum and their nearest faces were displaced horizontally by 15.1 cm from the suspension fiber axis. Arrows show the directions and relative magnitudes of the spins in configuration 4Ha. Configuration 2H omitted sources 2 and 4.

(the orbital g factor vanishes) so that the shields, which attenuate B, do not have an appreciable effect on V_1, V_2, and V_3.

Although the pendulum has essentially no external magnetic field it does have a substantial total angular momentum $\boldsymbol{J} = -\boldsymbol{S}$. This allowed us to use the observed Coriolis torque from earth's rotation to calibrate the net number of polarized spins in the pendulum and to measure the spin density of $SmCo_5$ (see [5] for details).

We used this same idea to construct 4 spin sources whose geometry is shown in Figs. 1 and 2. The magnetic fluxes from 12.7 cm × 5.08 cm × 2.54 cm stacks of $SmCo_5$ magnets were returned by magnet-iron yokes whose outer dimensions were 19.05 cm × 5.08 cm × 10.16 cm. Temporary coils wound on the yokes magnetized the iron to minimize the flux escaping from the magnetic circuits. The sources were then surrounded by 0.15 cm thick high-permeability shields that reduced the external fields to less than 10 mG. As the magnetization in iron, as well as Alnico, comes from polarized electrons, each $SmCo_5$ spin source provided a net polarization of 6.0×10^{24} spins.

We took data with two sources oriented horizontally on opposite sides of the pendulum (configuration 2H), and with 4 sources arrayed in horizontal or vertical pairs (configurations 4H and 4V) as shown in Figs. 1 and 2. These provided configurations with no sensitivity to some or all of the three potentials, or else changed the magnitude and direction of the torque from a given interaction, as listed in Table I. Over a period of 40 weeks, data were acquired with 16 variants of configuration 2H and 20(8) variants of configuration 4H(4V). The sources were mounted on a rotatable platform; this allowed us to check for consistency and possible systematic errors by acquiring essentially equal amounts of data in pairs of runs with two opposite azimuthal orientations of the source arrays. Our science signal was the difference between the two orientations. This eliminated lab-fixed systematics effects. However, magnetic or gravitational systematics associated
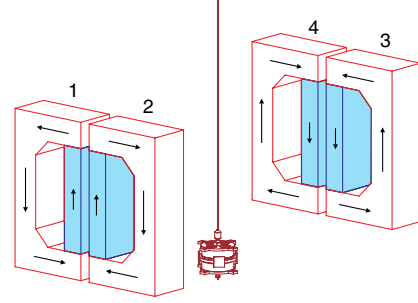

FIG. 2 (color online).   Scale drawing of the spin pendulum and the spin sources in configuration 4V. Arrows show the directions and relative magnitudes of the spins in configuration 4Va. Pairs of sources lay in a plane with their adjacent edges of the cores separated by 2.5 cm. Their edges facing the pendulum were displaced by 18.6 cm from the suspension fiber. The bottoms of the source cores were 2.0 cm above the pendulum.

with the spin sources themselves did not cancel. We checked for these effects by taking data with selected sources reoriented (configurations 4Hb and 4Hd) to reverse the directions of their magnetizations and gravity gradients. In Table I, configuration 4Ha is the *sum* of the configuration shown in Fig. 1 with one having the same spin orientations but with sources 1 and 3, as well as sources 2 and 4, interchanged. Configuration 4Hd represents the *difference* of those two configurations; this null combination probed for systematic effects from stray transverse magnetic fields.

Interactions V_1, V_2 or V_3 will modulate the rotating pendulum's energy as $E(t) = \hat{\boldsymbol{\sigma}}_p \cdot \boldsymbol{\beta}_s = \beta_s \cos[\phi_\beta - \phi_p(t)]$, where $\boldsymbol{\sigma}_p$ is the instantaneous orientation of the pendulum's net spin (determined by the turntable angle) and $\boldsymbol{\beta}_s$ depends on the source array configuration, the interaction involved, and the numbers of spins in the

TABLE I.   Some source orientations used in this work and their sensitivities to V_1, V_2, and V_3. N refers to the spin directions shown in Figures 1 and 2, R denotes the opposite orientation where the sources were rotated by 180 degrees about a vertical axis. N^* refers to the case where sources 1 and 3 and sources 2 and 4 were interchanged. The three rightmost columns show the direction of $\boldsymbol{\beta}$ for the V_1, V_2, and V_3 interactions with $m_b c^2 < 1.8$ μeV.

Configuration	Source				Sensitivity		
	1	2	3	4	V_1	V_2	V_3
2Ha	N		N		$-y$	$-x$	$-y$
2Hb	N		R		null	null	null
4Ha	N	N	N	N	$-y$	$-x$	$-y$
4Hb	N	N	R	R	null	null	null
4Hc	N	R	N	R	$+x$	$-y$	$+x$
4Hd	N^*	N^*	N^*	N^*	null	null	null
4Va	N	N	N	N	null	$+y$	$-x$
4Vb	N	N	R	R	null	null	null

pendulum and sources. The azimuthal angles ϕ_p and ϕ_β are defined with respect to x, where x is the horizontal projection of the vector pointing from the center of the pendulum to the midpoint of source 1 (or the 1–2 source pair), z points up and $y = z \times x$. It is clear from the symmetries of the source arrays that $\boldsymbol{\beta}_s$ must point either along (or against) x or y. The energy modulation created a torque $N = -\partial E/\partial \phi_p$ that twisted the pendulum by a very small angle $\theta(t)$ that was measured with a corotating optical system. The twist signal was decomposed into 1ω amplitudes $a_{\cos}$ and $a_{\sin}$ that varied as $\cos\phi_p(t)$ and $-\sin\phi_p(t)$ to obtain our fundamental experimental results $\beta_x = \kappa a_{\sin}$ and $\beta_y = \kappa a_{\cos}$, where $\kappa = 0.0185$ fN m/nrad is the torsional restoring constant of the suspension fiber. Results are shown in Fig. 3.

Systematic uncertainties from stray gravitational and magnetic fields of the sources were estimated as follows. The effect of stray magnetic fields was inferred by using Helmholtz coils to apply a flux of 360 Mx on the torsion balance's outermost magnetic shield. This produced a 1ω torque of 0.37 fN m on the pendulum. We conservatively assume that a source has a flux of 0.5 Mx (10 mG $\times$ 5 cm $\times$ 10 cm), that this entire flux intercepts the shield, and that two opposite sources have parallel stray fields; in this case the sources supply a total of 1 Mx to the shield. Scaling the 1ω torque by the flux ratio, we set our magnetic systematic at less than 0.001 fN m which we neglect in comparison to the statistical errors shown in Fig. 3. Asymmetries in placing the spin sources could produce a 1ω gravitational systematic. We measured the sensitivity of our pendulum to this using a calibrated Q_{21} source of 1.6 g cm^2, which produced a torque of 1.3 fN m. Detailed calculations of the gravitational fields of the spin sources indicated that a 5 mm misalignment of a single source would produce a Q_{21} field at the pendulum of 4.3×10^{-3} g cm^2, corresponding to a torque difference of 0.0035 fN m in a pair of runs, well below the typical statistical error per run pair of 0.03 fN m. Because the
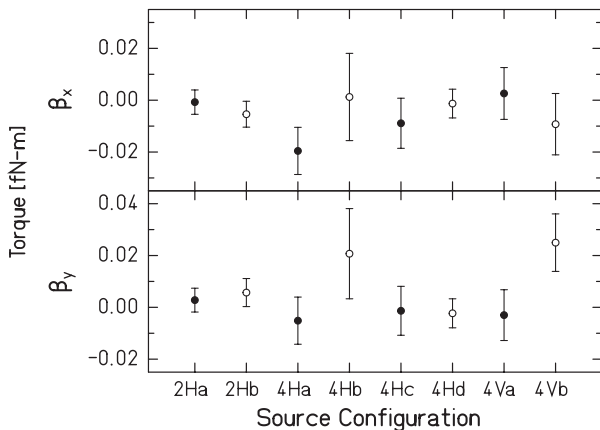

FIG. 3. Measured torques in each of our configurations. Hollow circles denote null configurations.
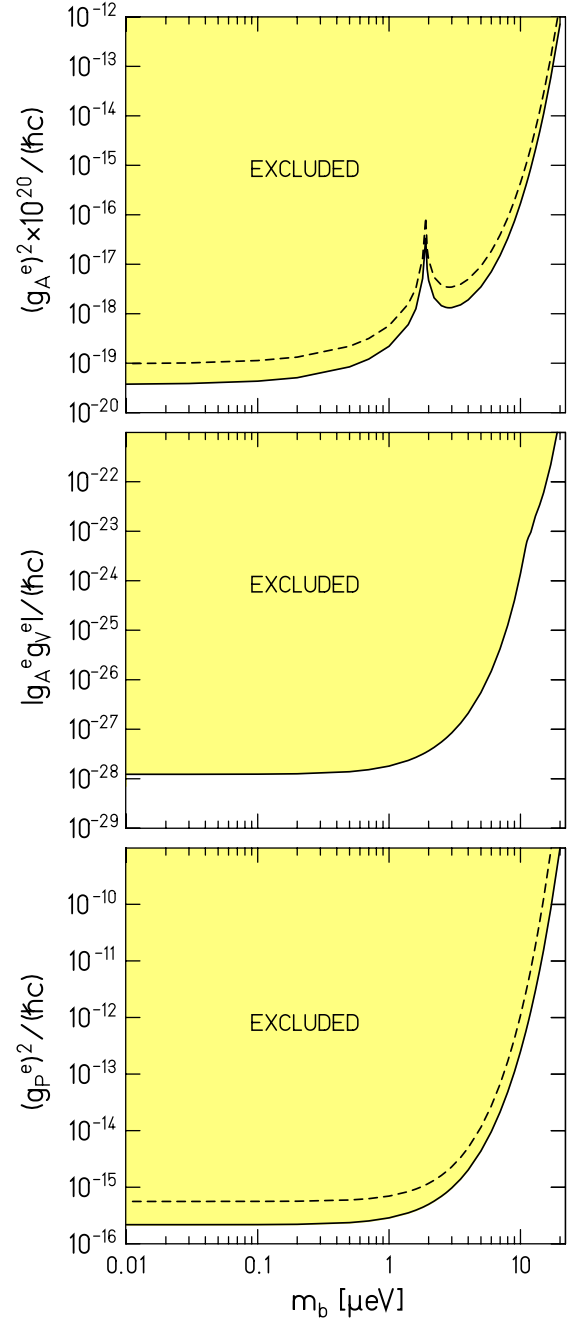

FIG. 4 (color online). 1σ constraints on couplings of exotic vector or pseudoscalar bosons to electrons. Solid and dashed lines show the one-interaction and three-interaction fits, respectively. Top panel: $(g_A^e)^2$. The dip at $m_b \approx 1.9$ μeV is caused by cancellation of the contributions of the upper and lower source components. The upper Alnico bar, with a large spin density, dominates for small m_b, while the lower and closer SmCo$_5$ bar with a small spin density, dominates for large m_b. Center panel: $|g_A^e g_V^e|$. The slope change at $m_b \approx 11.1$ μeV arises from competing contributions of the upper and lower source components. Because V_2's dependence on the source configuration is completely orthogonal to the other interactions (see Table I), the single and three-interaction constraints are identical. Bottom panel: g_P^e constraint extracted from our bounds on V_3.

TABLE II.   68.5% confidence bounds on coupling to electrons of bosons with $m_b \lesssim 0.1~\mu$eV.

Potential	Coupling	Value	
		e (this work)	n (Ref. [9])
V_1	$g_A^2/(\hbar c)$	$(-1.6 \pm 3.5) \times 10^{-40}$	1.5×10^{-40}
V_2	$g_A g_V/(\hbar c)$	$(9.2 \pm 6.5) \times 10^{-29}$	4.9×10^{-25}
V_3	$g_P^2/(\hbar c)$	$(-1.0 \pm 1.9) \times 10^{-16}$	7.3×10^{-9}

spin sources were removed and replaced between each pair of runs, the total gravitational uncertainty for each data set should average down and remain the same fraction of the statistical uncertainty. This again is negligible.

We computed the expected values of β_x and β_y for interactions V_1, V_2, and V_3 with coupling constant products $gg/(\hbar c) = 1$ using numerical integration routines. The pendulum was approximated as two parallel rectangular bars having the same height, mean-squared length, and mean-squared width as the $SmCo_5$ material in the pendulum and a spin density that gave the correct number of polarized electrons. This approximation is valid for $\lambda > R_p$ where $R_p = 9.3$ mm is the effective radius of magnetized material in the actual pendulum, so that we expect our calculated torques to be accurate for $m_b c^2 < 20~\mu$eV. Each source was approximated as a rectangular frame consisting of 4 trapezoidal slabs uniformly polarized with iron spin density, $\rho_{Fe} = (7.85 \pm 0.17) \times 10^{22}$ plus a superposed rectangular block representing the $SmCo_5$ with a spin density, $\Delta\rho = \rho_{Fe} - \rho_{SmCo} = (-3.66 \pm 0.08) \times 10^{22}$ [5]. The calculations were simplest for V_3 where the net contribution from a closed loop of spins vanishes and the torque arises entirely from the $SmCo_5$ blocks with effective spin densities $\Delta\rho$. The vanishing of the contribution from a closed loop of spins is a consequence of Stoke's theorem applied to a derivative-coupled potential. The V_1 and V_2 torques received contributions from the Alnico as well as the $SmCo_5$.

We fitted the data in Fig. 3 in three stages. First, we made the usual assumption that only 1 of the 3 interactions was present, allowing the coupling constant product to have an arbitrary sign; results are shown in Fig. 4 and Table II. Second, we assumed that all 3 interactions were present; these weaker constraints are shown as dashed lines in the figures. Finally, we constrained spin-1 bosons with real coupling constants g_V and g_A. Our constraints on g_A and g_V are interdependent as shown in Fig. 5.

It is worth noting that our limit $g_P^e/\sqrt{\hbar c} \lesssim 1.5 \times 10^{-8}$, the tightest existing laboratory result, is nevertheless much weaker than the astrophysical bound of $<3 \times 10^{-13}$ [10]. Hunter *et al.* [11] recently used our existing bound [5] on a preferred orientation of the spin pendulum relative to the spin polarization of the earth to constrain V_1, obtaining $g_A^2/(\hbar c) \lesssim 4 \times 10^{-47}$ for $m_b c^2 < 20$ feV. That limit is tighter than ours for masses less than ≈ 200 peV. Hunter
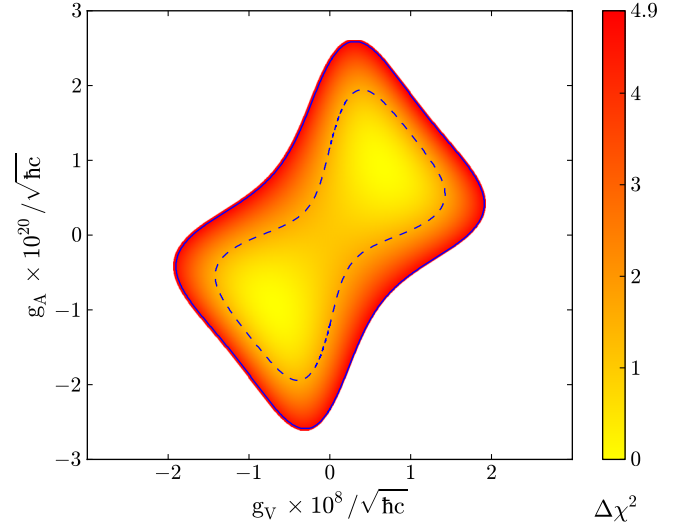

FIG. 5 (color online).   Constraints on axial and vector couplings g_A^e and g_V^e of spin-1 bosons with mass less than $0.1~\mu$eV. The solid and dashed contours correspond to 68.5% and 95.3% confidence levels determined from 10 000 simulated data sets.

et al.'s limit on V_2 is less stringent than ours except for $m_b c^2 \sim 100$ peV where it is comparably precise.

Analogous constraints on V_1, V_2, and V_3 interactions of neutrons have been reported by a Princeton group [9]. Their results are included in Table II.

We thank Bogdan Dobrescu for conversations that stimulated these measurements. The spin sources used in this work were built by C. E. Cramer. This work was supported by NSF Grant No. PHY0969199 and by the DOE Office of Science.

[1] E. G. Adelberger, J. H. Gundlach, B. R. Heckel, S. Hoedl, and S. Schlamminger, Prog. Part. Nucl. Phys. **62**, 102 (2009).
[2] J. E. Moody and F. Wilczek, Phys. Rev. D **30**, 130 (1984).
[3] B. A. Dobrescu and I. Mocioiu, J. High Energy Phys. 11 (2006) 005.
[4] V. A. Kostelecký and N. Russell, Rev. Mod. Phys. **83**, 11 (2011).
[5] B. R. Heckel, E. G. Adelberger, C. E. Cramer, T. S. Cook, S. Schlamminger, and U. Schmidt, Phys. Rev. D **78**, 092006 (2008).
[6] S. A. Hoedl, F. Fleischer, E. G. Adelberger, and B. R. Heckel, Phys. Rev. Lett. **106**, 041801 (2011).
[7] J. E. Kim, Phys. Rep. **150**, 1 (1987).
[8] R. T. Hammond, Rep. Prog. Phys. **65**, 599 (2002).
[9] G. Vasilakis, J. M. Brown, T. W. Kornack, and M. V. Romalis, Phys. Rev. Lett. **103**, 261801 (2009).
[10] G. Raffelt and A. Weiss, Phys. Rev. D **51**, 1495 (1995).
[11] L. Hunter, J. Gordon, S. Peck, D. Ang, and J.-F. Lin, Science **339**, 928 (2013).